DOI: 10.1002/ejic.201100217

Hybrid Architectures from 3D Aligned Arrays of Multiwall Carbon Nanotubes and Nanoparticulate $LiCoPO_4$: Synthesis, Properties and Evaluation of Their Electrochemical Performance as Cathode Materials in Lithium Ion Batteries

Jörg J. Schneider,*[a] Jayaprakash Khanderi,[a] Alexander Popp,[a] Jörg Engstler,[a] Hermann Tempel,[a] Angelina Sarapulova,[b] Natalia N. Bramnik,[b] Daria Mikhailova,[b] Helmut Ehrenberg,[b] Ljubomira A. Schmitt,[c] Lucangelo Dimesso,[c] Christoph Förster,[c] and Wolfram Jaegermann[c]

Keywords: Hybrid materials / Lithium-ion batteries / Electrochemistry / Nanotubes / Nanoparticles / Phosphoolevins

Hybrid materials composed of $LiMPO_4$ (M = Fe or Co) with multiwalled carbon nanotubes (MCNTs) were synthesized by tethering lithium phosphoolevins on isolated stochastically disordered MWCNTs as well as on ordered 3D MWCNT arrays via solution based impregnation routes. Ordered 3D arrays of MWCNT monoliths comprising MWCNTs with nominal tube diameters of 60 and 200 nm were synthesized by a catalyst free, template based method, with porous aluminum oxide (PAOX) acting as a template. Consecutive selective etching processes gave free standing aligned 3D carbon nanotube (CNT) architectures that were used as supporting cathode structures for electroactive $LiCoPO_4$. $LiCoPO_4$ nanoparticle suspensions derived from an ethanol based organic phosphate source turned out to be superior for the tethering of $LiCoPO_4$ nanoparticles onto the 3D aligned CNT arrays compared to an aqueous based tethering route, thus giving hybrid materials with better electrochemical battery performance compared to materials generated by the latter method. Li ion extraction within the ordered 3D CNT/$LiCoPO_4$ composites seems to be a two-step process and the Li intercalation a one-step process, highlighting the enhanced kinetics of the Li insertion process in the 3D CNT/Li_xCoPO_4 composite in comparison to a particulate mixture of Li_xCoPO_4 that is typically present in a conventional carbon/$LiCoPO_4$ cathode composite system.

Introduction

The integration of CNTs into micro components is one of the main challenges concerning their future technological implementation in highly organized device architectures.[1] The vertical alignment and integration of CNTs from nanosized, via microsized, into macrosized arrays allows for the use of such 1D structures as high surface area materials. The creation of such assemblies enables the directional tethering of functional nanoparticles alongside individual CNTs within such CNT arrays, which is interesting for advanced materials applications in the energy field e.g. for solar cells, Li ion batteries and catalytic converters.[2–4] Recently, we showed the potential of such massively integrated 3D ordered CNTs for the generating of a new type of microsized reactor based solely on CNTs and its subsequent application in catalysis.[5] The tethering of catalytically active metals (e.g. Au, Pd, Pt) as well as oxidic nanoparticles (e.g. ZnO, CeO_2) with a high ratio of coverage on the outside of CNTs is of utmost importance in such devices.[2,6] Demands for advanced energy storage devices have increased significantly each year during the past decade.[7,8] Li ion technology relies on a rich and versatile chemistry that has leaded to a wide range of attractive materials for positive electrodes (e.g. $LiCoO_2$, $LiMn_2O_4$, $LiFePO_4$), and several cathode materials that exhibit promising electrochemical performances. $LiFePO_4$ was introduced in the late 1990s, and is particularly interesting due to its low cost and environmental compatibility.[9] For $LiFePO_4$, the discharge voltage is about 3.4 V vs. Li/Li^+ and the capacity fade can be small even after several hundred cycles. Its reversible capacity can be up to 140–150 mA h/g, which is close to the capacities of other currently commercially used cathode materials. However, one of the main drawbacks of $LiFePO_4$ that is preventing its broader commercial exploitation is its low electronic conductivity and low Li ion diffusivity across the $LiFePO_4/FePO_4$ interface during charge/discharge process cycles.[10] One of the most promising solutions to overcome the inherently bad conductivity of $LiFePO_4$ is the introduction of thin carbon coatings onto the

[a] Eduard-Zintl-Institut für Anorganische und Physikalische Chemie, Fachbereich Chemie, Technische Universität Darmstadt, Petersenstraße 18, 64287 Darmstadt, Germany
Fax: +49-6151-16-3470
E-mail: joerg.schneider@ac.chemie.tu-darmstadt.de
[b] Institut für Komplexe Materialien, IFW Dresden, Helmholtzstr. 20, 01069 Dresden, Germany
[c] Fachbereich Material- und Geowissenschaften, Technische Universität Darmstadt, Petersenstraße 23, 64287 Darmstadt, Germany

surface of the active material.[11] Such carbon coatings with different material properties can be prepared in a number of ways.[11–15] In addition to the type and morphology of the carbon coating, its degree of connection with the $LiFePO_4$ cathode material determines the electrical conductivity and the charge transport within the composite cathode. CNTs provide a unique opportunity for realizing such an improvement, since they display good electrical conductivity along their tube axis and a high surface area suitable for tethering of electroactive compounds, especially those with nanoparticulate morphology.[16–18] Moreover, they can be synthesized by a number of different approaches and are even available in technological relevant amounts. When depositing electroactive compounds onto the surface of CNTs a number of positive effects on the electrochemical performance of such a coaxially aligned composite electrode configuration can be envisaged: (i) an improved overall electronic conductivity of the composite; (ii) a directed electrochemical accessibility combined with a high ionic conductivity as the need for additional agglomerative and conductive binder components is avoid; (iii) well directed 1D conductive pathways due to the perfect coaxial alignment of the CNTs, which enhances the Li ionic conductivity and transport within the composite; (iv) a reduced diffusion length due to the nanometric length scale of the arrays; (v) a better overall composite stability under oxidative conditions, and the structural changes experienced by the oxide during the charge/discharge cycles can be compensated for by the mechanically highly flexible CNTs. Consequently research into composite materials composed of CNTs and electroactive compounds has been intense; NiO,[4] MnO_2,[3] Fe_2O_3,[19] V_2O_5,[4] RuO_2[4] and SnO_2[4] have been deposited on the walls of CNTs and these materials have been studied in the context of supercapacitors and Li ion batteries.[17,19,20,21] Micrometer sized CNT/$LiMPO_4$ 3D architectures could act as supports and as anisotropic electrical conductors offering an unidirectional conductivity pathway, however, they not been studied to date. Such hybrids may prove especially interesting since their high conductivity is essential for improved cyclability, such materials also offer enhanced electrode stability by avoiding the need for high contents of carbon binder materials to act as electronic conducting components in such cathodes. Additive components may do the following: (i) react destructively under cell operation; (ii) confine the possible load of electroactive material to the battery electrode surface. Indeed, for charged $LiCoPO_4$ based battery cathodes, a release of oxygen at elevated temperatures has been reported.[20] Thus, CNTs based cathodes could certainly offer improved thermal, oxidative and mechanical stability paired with better electrical conductivity. The careful tailoring of both the CNT cathode architecture and the morphology of the active lithium–phosphoolevin material, which is the Li storage material, may be a crucial factor for improving the cathode performance in order to deliver high capacity and good cyclability, and as such these materials deserve further research.

Herein we report for the first time the preparation, characterization and electrochemical performance of 3D MWCNT/$LiCoPO_4$ nanocomposites of micron to millimeter dimensions containing 3D CNT array structures. Nanocomposites with two different CNT base architectures were studied. On the one hand, stochastically distributed CNTs acted as the supports for tethering of the electroactive $LiCoPO_4$ olevin compound, resulting in a felt-like CNT/olevin composite. On the other hand, 3D aligned CNT architectures with uniform and unidirectional morphologies and of micrometer dimensions were created, the well arranged CNTs of which formed a base structure for the attachment of the $LiCoPO_4$ olevin. This results in a highly ordered 3D CNT/phosphoolevin composite array. Such arrays containing CNTs with nominal diameters of 60 and 200 nm were employed in our studies.

Results and Discussion

Formation of Monolithic 3D CNT Structures with Different CNT Pore Diameters

A schematic representation of the overall process employed in the formation of the 3D CNT/$LiCoPO_4$ hybrid materials is shown in Figure 1. The porous template is obtained by anodic oxidation of aluminium under controlled electrochemical conditions (Figure 1, a).[22,23] The template is then filled with CNTs with an appropriate diameter by employing an uncatalyzed chemical vapour deposition

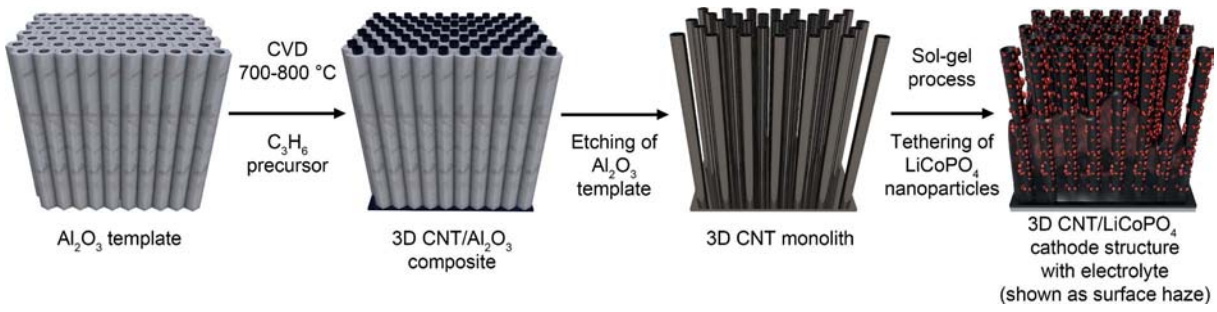

Figure 1. Schematic representation of the preparation procedure for 3D aligned $LiMPO_4$/CNT composite structures. First, CNTs were deposited by CVD into porous alumina templates (with nominal pore size diameters of 60 and 200 nm). After etching of the alumina template, the freestanding CNT array is dipped in and infiltrated by a $LiCoPO_4$ sol to tether the electroactive precursor particles to the CNT surfaces. The cathode structure is then calcined, infiltrated with the electrolyte, and built into the battery cell architecture.

(CVD) process conducted at 800 °C for about 20 min with ethylene or propylene as the precursor gas (Figure 1, b).[5] This process is followed by plasma and wet chemical etching to remove the template, which results in a freestanding 3D CNT monolithic structure (Figure 1, c). The 3D CNT monolithic structure is then immersed under controlled conditions for a period of time in a sol of $LiMPO_4$ to obtain a composite that can then be calcined to obtain the final 3D CNT/$LiCoPO_4$ hybrid electrode. In this hybrid cathode structure the CNTs are freestanding and are attached at both ends to a carbon layer.[5] For a better infiltration of the electroactive $LiMPO_4$ (M = Fe) nanoparticle sols, it is desirable to obtain a cathode device configuration in which one of the carbon layers is selectively detached from the CNTs (see Figure 1). This would allow for a dense tethering of the electroactive nanoparticles on the CNT surface, as well as intensive impregnation of the electrolyte suspension within the 3D CNT block array. Scanning electron microscopy (SEM) pictures of a freestanding monolithic CNT block with CNTs with nominal diameters of 60 (upper row) and 200 nm (lower row) that were obtained after complete etching of the alumina template are depicted in Figure 2.

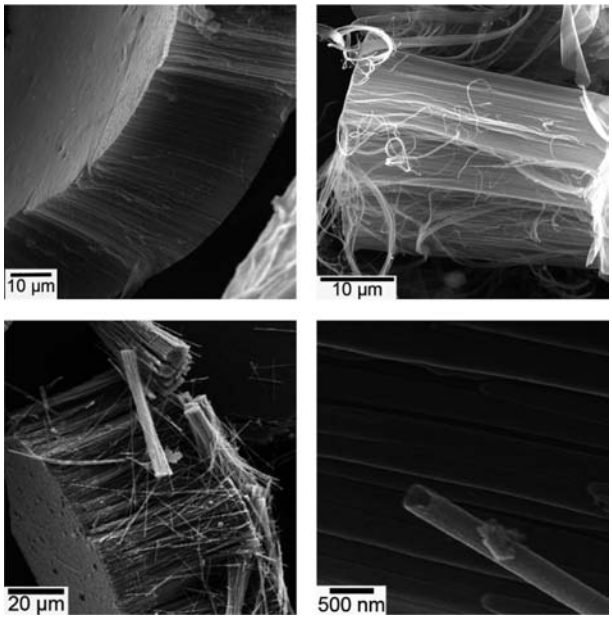

Figure 2. SEM micrograph showing the block arrangement of the 3D CNT block array. The nominal CNT diameter is 60 ± 5 nm. Upper left: complete CNT block structure with top and bottom layers; upper right: side view of the block showing the parallel arrangement of the CNTs within the block, this image was recorded at high magnification; lower left: side view of the parallel arrangement of the 3D CNT block structure comprising CNTs that are 200 nm in diameter; lower right: high magnification SEM image showing the morphology of individual CNTs within the 3D block structure (CNTs are 200 nm in diameter).

Figure 3 shows transmission electron microscopy (TEM) micrographs of individual CNTs with nominal diameters of 60 nm that were unhinged from a 3D block structure by ultrasonification. These images show that the CNT block arrangements are composed of well aligned CNTs, the lengths of which are determined by the thickness of the alumina template. The MWCNTs obtained by this process are graphitized (Figure 3, c), however there is a certain amount of disorder within their graphitic domains that is restricted to relatively small areas (Figure 4), this is typical for MWCNTs generated by this process.[24] However, such MWCNTs show good electrical conductivity,[25] and in addition, their short order graphitic domains gives them a high degree of mechanical flexibility. Moreover, the additional defect sites will allow for the straightforward chemical functionalization of such MWCNTs.

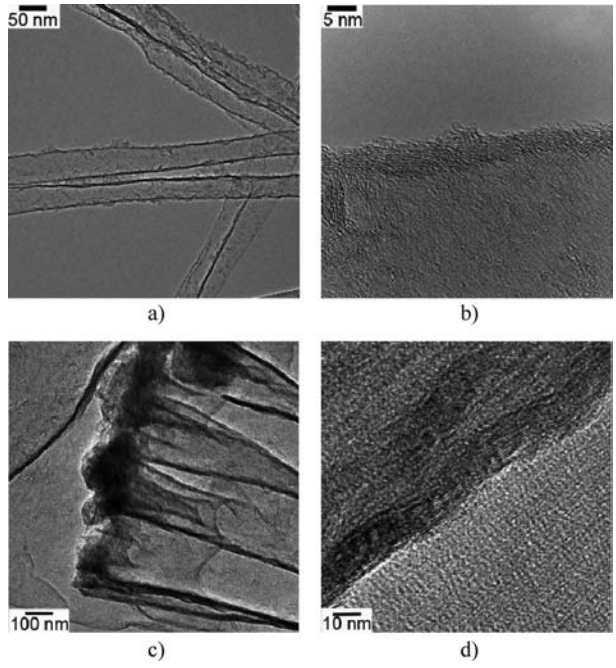

Figure 3. TEM micrographs of CNTs with nominal diameters of 60 nm (a and b) and 200 nm (c and d). These images show the graphitization of individual CNTs within the 3D CNT block structure. The samples were obtained by unhinging CNTs from the block structure by ultrasonification.

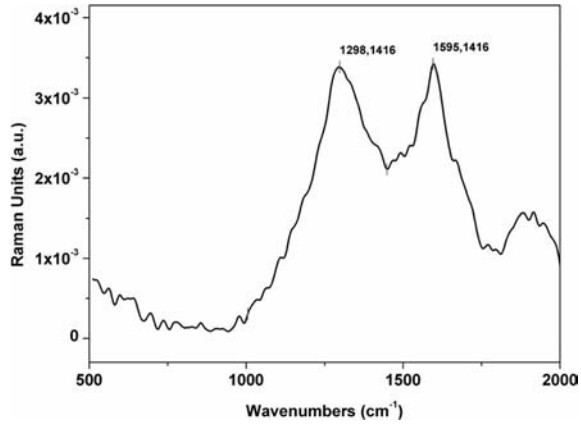

Figure 4. Raman spectrum of a 3D CNT block structure showing the characteristic D and G signal pattern.

The partially graphitic and defect rich nature of such MWCNTs (200 nm in diameter) within a 3D CNT block

structure has been proven by Raman spectroscopy.[24] Typically two peaks in the spectrum, the so called D and G modes, are characteristic of such MWCNTs. Figure 4 shows a Raman spectrum of a 3D CNT array comprising CNTs that are 60 nm in diameter, which was employed in our studies. The D mode at 1298 cm^{-1} is due to defect structures associated with the disorder of the curved graphene layers. The G peak at 1595 cm^{-1} (tangential E_{2g} mode) corresponds to the fundamental mode for the crystalline graphite areas. A strong D mode corresponds to a low degree of graphitic ordering (i.e. disorder).

The 3D CNT array structures reported herein can be obtained in sizes ranging from several square microns to several square millimeters, which allows for their direct integration into future micro devices.[5,26]

Functionalization of CNTs within the 3D CNT Monolithic Structure

A straightforward chemical functionalization of the 3D CNT monolithic structures can be realized with concentrated mineral acids viz. HNO_3 and H_2SO_4. Small pieces of the intact monolithic CNT species (Figure 2, a and b) were heated in concentrated HNO_3 at 80 °C and at 140 °C, and in a mixture of HNO_3/H_2SO_4 (1:3) at 70 °C. After washing and drying, the 3D CNT monolith structures were characterized by infrared spectroscopy (IR) and SEM in order to investigate their degree of functionalization (IR) and structural integrity (SEM). The IR spectra of the HNO_3 treated samples are shown in Figure 5.

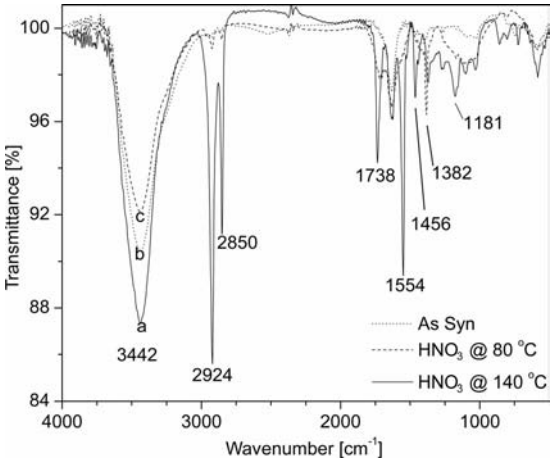

Figure 5. IR spectra of a 3D CNT block structure: (a) before acid treatment; (b) after HNO_3 acid treatment at 80 °C; (c) after HNO_3 acid treatment at 140 °C.

The spectra depicts absorption bands for COOH at $\tilde{\nu}$ = 1738 cm^{-1}, for OH at $\tilde{\nu}$ = 1181 cm^{-1}, for CH_2 in the range $\tilde{\nu}$ = –2900–2850 cm^{-1} and for the N–O stretching vibration at $\tilde{\nu}$ = 1550 and 1382 cm^{-1}. The intensities of these bands increase as the temperature employed in the functionalization procedure is increased. An SEM image of the 3D CNT monolith after functionalization with conc. HNO_3 at 140 °C (Figure 6) indicates the morphological integrity of the structure after etching. The block arrangement of the 3D monolith is completely retained after exposure to these conditions. In contrast to these results, treatment of the 3D CNT monolithic structure with a mixture of HNO_3/H_2SO_4 (1:3) at 70 °C results in the complete destruction of the CNT monolith, indicating that the optimum conditions for functionalization of the 3D CNT monolith is treatment in HNO_3 at 140 °C.

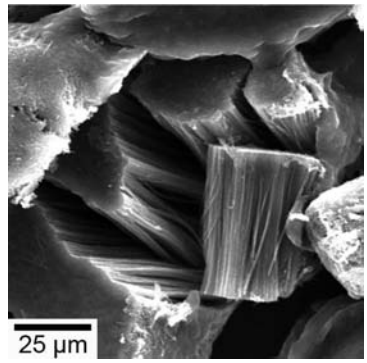

Figure 6. SEM micrograph of a typical 3D CNT block structure after HNO_3 treatment at 140 °C.

In order to allow for the most effective infiltration of the $LiMPO_4$ sol particles into the 3D aligned CNT block structure, we developed a selective etching procedure using a pure oxygen plasma to remove one of the top carbon layers from the CNT nanostructure. For this procedure we used the PAOX/CNT composite obtained after CNT infiltration of the alumina template by the CVD method. By exposing one side of the composite to the oxygen plasma, a single top carbon layer can be removed selectively from the monolith structure, while maintaining the backside carbon layer for mechanical stabilization of the composite. After plasma etching the PAOX template can be completely removed by an additional wet chemical etching step with HF. This process can be controlled by selecting different time intervals for the etching process, and it is possible to retain an alumina base at the bottom of the 3D CNT monolith structure, which provides further mechanical stabilization of the 3D monolith. Figure 7 depicts different SEM views of the 3D monolithic CNT structures (the CNTs have nominal diameters of 60 and 200 nm and have been subjected to oxygen plasma etching, followed by wet chemical HF etching leading to the controlled and selective removal of the PAOX template).

The general suitability of the voids in such a 3D CNT monolith structure for the impregnation and tethering of nanoparticles to the individual CNTs inside the CNT monolithic block structure has recently been demonstrated by us for zinc oxide nanoparticles as well as for polymers like polystyrene and poly(methyl methacrylate) (PMMA).[2,27] Thus, the outer surface of the individual MWCNTs in the CNT block structure is completely accessible. Furthermore, the propensity of the individual MWCNTs within the CNT block structure for charge transport has been verified by the spontaneous reduction of Au^{3+} and Pt^{2+} solutions to

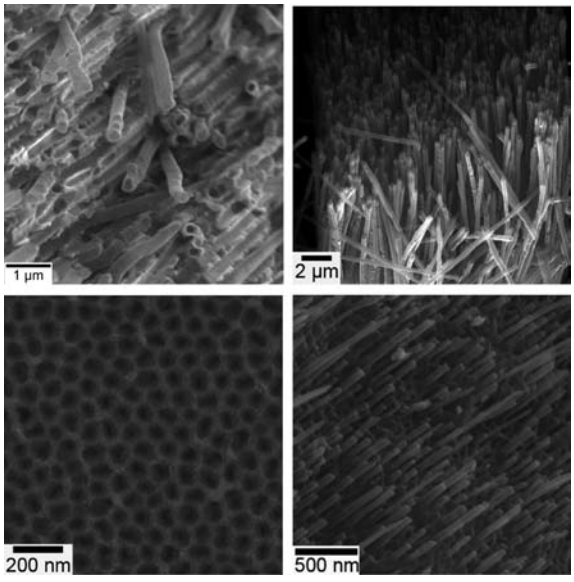

Figure 7. SEM images showing the extent of template etching after the top carbon layer was removed from the 3D CNT monoliths, and the resultant structures treated with HF. Upper left: CNTs 60 nm in diameter; upper right: CNTs 200 nm in diameter; lower left: oxygen plasma etched top carbon layer of the 3D CNT block structure; lower right: 3D CNT block structure after partial etching of the alumina template.

form Au^0 and Pt^0 nanoparticles on the surface of the individual CNTs comprising such a 3D CNT monolith.[2] These independent experiments provide valuable evidence for the capability of individual CNTs within the ordered 3D CNT monolith structure to act as conductive materials for battery applications.

Synthesis and Characterization and Electrochemical Performance of Ordered 3D CNT/$LiCoPO_4$ Composite Cathodes

Ordered 3D CNT/$LiCoPO_4$ composites were obtained by immersing the 3D CNT monoliths for 48 h in 5 mL of a hydrolyzed $LiCoPO_4$ nanoparticle precursor solution (e.g. 0.1 M). After removing the carbon monoliths from the solution the composites were heat treated with different temperature regimes. Some admixture of metallic cobalt was observed in the final 3D CNT/$LiCoPO_4$ composites after they were annealed in Ar at 650–700 °C (Figure 8, a). The formation of metallic Co might be due to the strong reductive properties of the CNTs, and the extent of reduction depends on the reaction time employed for the impregnation step. On the other hand, if the calcination of the precursor particles is first performed at 500 °C in air, followed by a temperature increase to 700 °C under Ar (for 12 h), single phase $LiCoPO_4$ with a minor amount of Co_3O_4 impurity (cubic phase, Figure 7, b) is obtained. The same results were obtained for the synthesis of stochastically ordered MWCNT/$LiCoPO_4$ composites.[28] The morphology of the former CNT composite displays a regular arrangement of individual CNTs within the 3D block array, without formation of $LiCoPO_4$ agglomerates, and an average $LiCoPO_4$ particle size between 50 and 70 nm (Figure 9).

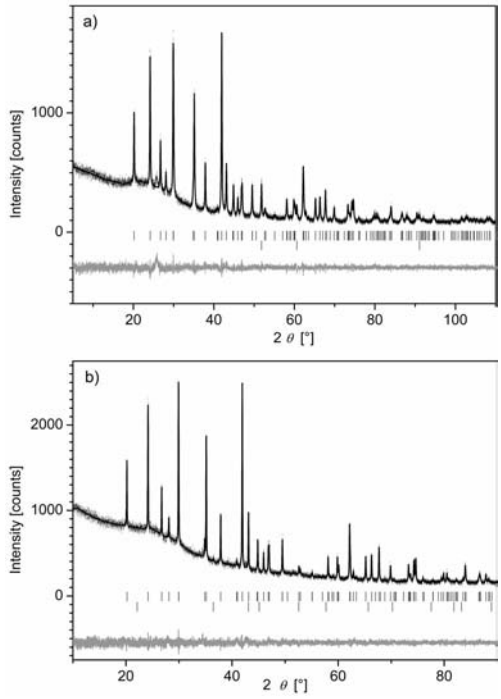

Figure 8. (a) Measured and calculated X-ray powder diffraction patterns for 3D CNT/$LiCoPO_4$ after treatment at 700 °C in an Ar flow, also shown is the difference curve for the two patterns (Co-$K_{\alpha 1}$ radiation). The second phase (lower line of reflection marks) corrsponds to metallic Co; (b) measured and calculated X-ray powder diffraction patterns for 3D CNT/$LiCoPO_4$ composite after treatment at 500 °C in air for 2 h followed by heating at 700 °C in Ar for an additional 12 h. Also shown is the difference curve for the two patterns (Co-$K_{\alpha 1}$ radiation). The fitted profile at the bottom corresponds to the cubic phase of Co_3O_4.

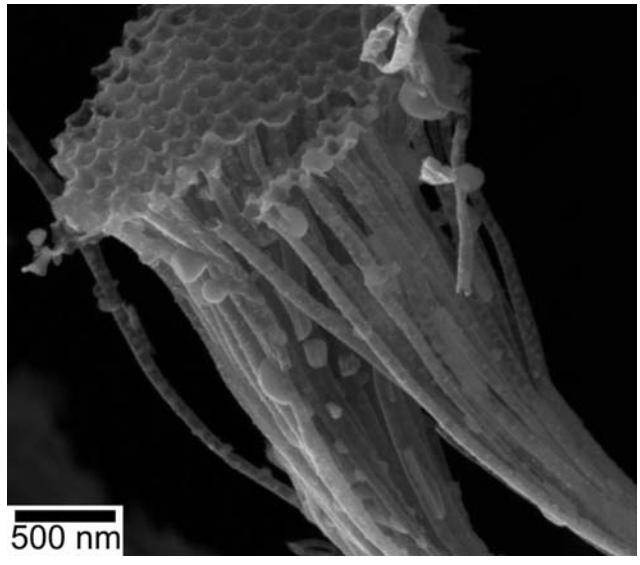

Figure 9. SEM micrograph of an ordered 3D CNT/$LiCoPO_4$ composite containing CNTs with a norminal diameter of 60 nm. The phosphoolevin particles are covering the outside of the CNTs fairly homogeneously, although occasionally larger agglomerates are visible.

Ordered 3D CNT/$LiCoPO_4$ composites, with individual CNTs with diameters of about 200 nm, were obtained by using large alumina templates (200 nm Whatman, Anopore) in the CNT synthesis, followed by etching of the template, and finally filling of the 3D CNT array structure by a similar impregnation procedure to that mentioned above.

SEM characterization of the 3D CNT/$LiCoPO_4$ array containing CNTs that are 200 nm in diameter revealed tethering of the $LiCoPO_4$ nanoparticles on the outside of the CNTs (interstitial volume of the 3D CNT block arrays) as well as on the interior of the CNTs indicating a partial filling of the CNTs (Figure 10). It is interesting to note that the deposited $LiCoPO_4$ nanoparticles have a broad size distribution, which suggests that initial control of the particle size is of utmost importance for ensuring a homogeneous deposition of the electrocactive species within the 3D CNT/$LiCoPO_4$ array.

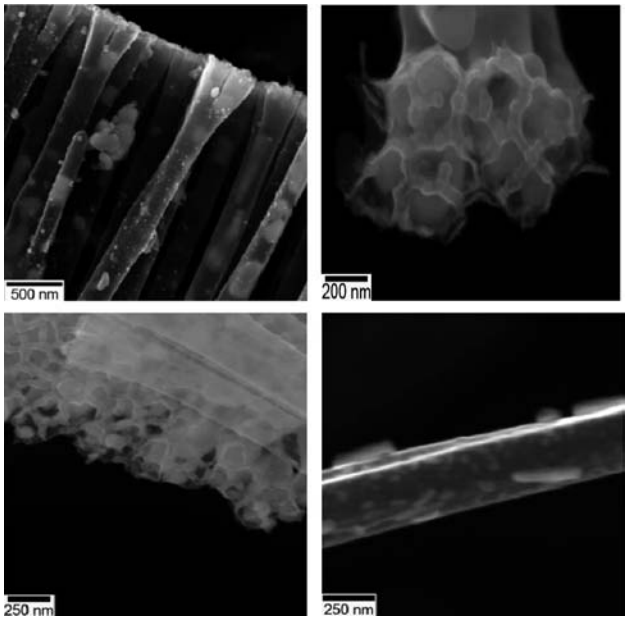

Figure 10. SEM image of an ordered 3D CNT/$LiCoPO_4$ (comprising CNTs with a nominal pore diameter of 200 nm) composite, the morphology shows tethering of the $LiCoPO_4$ particles on the CNT surface (upper left and lower right) as well as in the interiors of the individual CNTs of the 3D CNT block structure (upper right and lower left).

TEM and high resolution TEM investigations of the 3D CNT/$LiCoPO_4$ composites (with CNTs 60 nm and 200 nm in diameter) were performed in order to study the degree of loading of the $LiCoPO_4$ nanoparticles inside and outside the CNT structures. Samples were obtained by unhinging individual CNT structures from the 3D CNT/$LiCoPO_4$ block arrays by ultrasonification. As indicated by the SEM studies, and in full accord with these (see Figure 9), the TEM images prove that loading of the $LiCoPO_4$ particles occurs on the outside and inside surfaces of the individual CNTs [Figure 11 (a and b) shows images for CNTs 200 nm in diameter]. The outside surface coverage (loading) of the $LiCoPO_4$ on the CNTs seems to be higher for the 200 nm CNTs compared to the 60 nm CNTs (see Figure 11, part a vs. c). This fact is in full accord with the significantly diminished CNT inter-distances in the 3D CNT block arrays of the 60 nm vs. 200 nm CNTs, which may result in hindered sol infiltration into the two different CNT array structures during the impregnation step; especially when one keeps in mind that the range of diameters for the $LiCoPO_4$ particles is comparable to the tube diameter and the CNT inter-distances for the 3D arrays comprising CNTs 60 nm in diameter. The $LiCoPO_4$ particles are highly crystalline (indicated by the lattice fringes associated with the $LiCoPO_4$ particles in Figure 11f). The particles show intimate contact with the graphitic CNT wall structure of the 200 nm CNTs as well as for the 60 nm CNTs (Figure 11b and Figure 11f). Furthermore, it is interesting to note that the electrostatic ζ-potentials of the $LiCoPO_4$ nanoparticulate sol and the 3D CNT nanotube material, both in ethanol at 25 °C, exhibit opposing values of 3.3 mV for the phosphoolevin particles, and for the CNTs a negative surface charge of –6.2 mV was determined. This explains the high chemical affinity of the

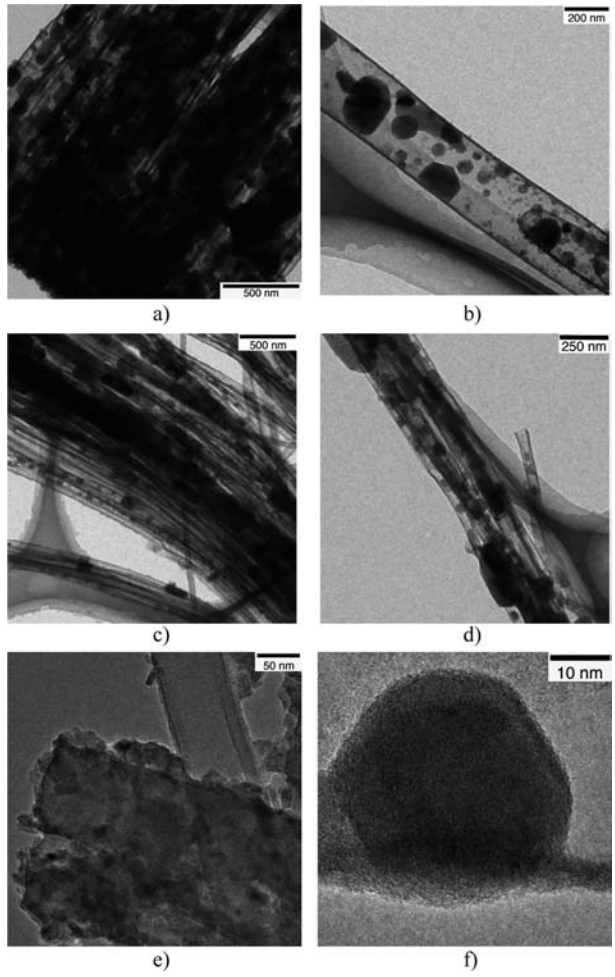

Figure 11. TEM micrographs of individual CNT/$LiCoPO_4$ composite structures that were unhinged from intact 3D aligned CNT/$LiCoPO_4$ composite block structures by ultrasonification: 200 nm CNTs are shown in a and b, and 60 nm CNTs are shown in c–f. The tethering of the crystalline $LiCoPO_4$ particles onto the CNT walls is clearly visible for CNTs of both diameters, 200 nm (b) and 60 nm (f).

inorganic $LiCoPO_4$ particles for the MWCNTs. The negative surface charge of the CNTs is due to a significant functionalization of the CNT tube surface with OH and COOH groups, and is in sound agreement with the IR and Raman spectroscopy results. Further acid functionalization e.g. with HNO_3 or gas phase plasma functionlization (air or O_2) causes this effect to become even more pronounced.

Electrochemical Characterization of Ordered 3D CNT/$LiCoPO_4$ Composite Cathodes

Good electrochemical performance for composite electrodes composed of carbon black and $LiCoPO_4$ has been reported.[29,30] We have studied the electrochemical performance of our two ordered 3D CNT/LiCoPO4 composite materials that comprise CNTs with two different diameters.

Cyclic voltammograms of the 3D ordered arrays comprising CNTs with nominal diameters of 60 and 200 nm but without active material (Figure 12) show the occurrence of irreversible oxidation processes at ca. 5.2 V vs. Li^+/Li, which are very pronounced in the curves for the first cycles and could correspond to the oxidation of electrolyte and/or the CNTs. Additional oxidative peaks at about 4.85 V for CNTs with a nominal diameter of 60 nm and at 4.2 V for those with a nominal diameter of 200 nm, which are very pronounced in the curves for the first cycles, could be attributed to the parasitic oxidation of the CNTs (Figure 10, b).

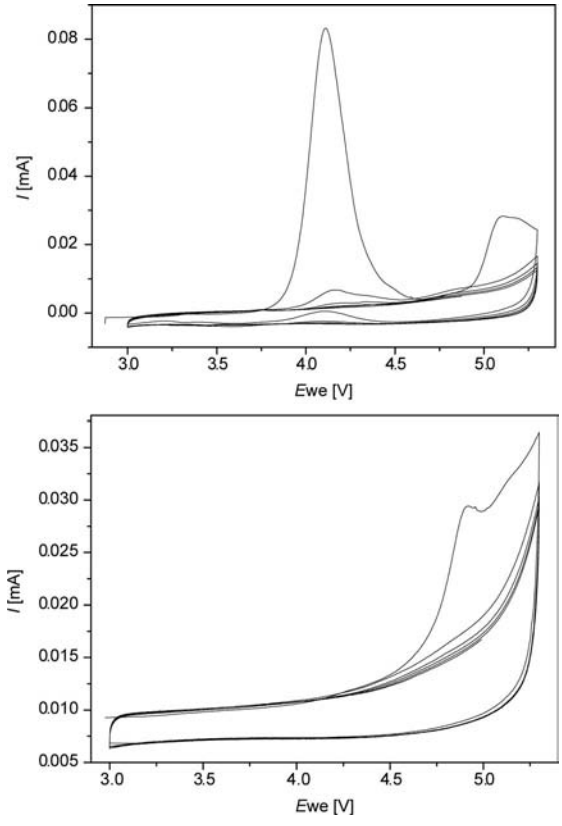

Figure 12. Cyclic voltammograms for block arranged 3D CNTs that have been processed at 700 °C in argon and do not contain electroactive $LiCoPO_4$ phosphoolevin. Top: 3D CNT block comprising CNTs with a nominal diameter of 60 nm; bottom: 3D CNT block comprising CNTs with a nominal diameter of 200 nm.

Figure 12 shows results of the cyclic voltammetry (CV) studies of the ordered 3D CNT/$LiCoPO_4$ composites containing CNTs with a nominal diameter of 60 nm that were performed over the 3–5 V potential range under ambient conditions. The peak corresponding to the oxidation of the 3D CNT array may be hidden in the curve for the first charge cycle of the 3D CNT/$LiCoPO_4$ composite.

The electrochemical measurements of the 3D CNT/$LiCoPO_4$ composites reveal that they display good reversibility and structural stability during electrochemical cycling. Two pronounced oxidative peaks at 4.8 and 5.0 V but only one reductive peak at 4.7 V are observed in their voltammograms, indicating a complicated mechanism for Li removal/insertion into the nanoscaled electroactive $LiCoPO_4$ particles that are tethered onto the 3D CNT monolith structures. The stepwise appearance/disappearance of two Li deficient phases of $LiCoPO_4$, with the same olivine-like structure but different Li ion contents, that form upon electrochemical lithium extraction/insertion has been confirmed by in situ synchrotron diffraction experiments. The Li deficient phases identified in these experiments were $Li_{0.6(1)}CoPO_4$ and $CoPO_4$.[32] It is generally known that different synthesis routes lead to different $LiCoPO_4$ morphologies, which in turn influence the electrochemical Li extraction/insertion process.[31] Based on these studies, the Li ion extraction for the ordered 3D CNT/$LiCoPO_4$ composites containing CNTs with a nominal diameter of 60 nm seems to be a two-step process and the Li intercalation a one-step process. Note that the coexistence of $LiCoPO_4$, $Li_{0.6(1)}CoPO_4$ and $CoPO_4$ in the intermediate state of charge does not represent an equilibrium state according to Gibbs' phase rule. Therefore, the observed one-step character of the discharge process hints at enhanced kinetics for the Li insertion process within the 3D CNT/Li_xCoPO_4 composite when compared to a particulate composite mixture containing carbon/Li_xCoPO_4 that is typically used in a conventional carbon/binder/$LiCoPO_4$ cathode system.

The voltammogram from galvanostatic cycling at C/10 of an ordered 3D CNT/$LiCoPO_4$ composite containing CNTs with a diameter of 200 nmrevealed a pronounced plateau at 4 V vs. Li^+/Li, (Figure 13), which corresponds to the para-

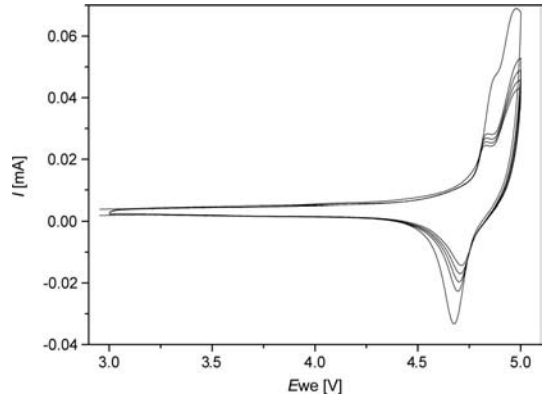

Figure 13. Cyclic voltammograms for a 3D CNT/$LiCoPO_4$ composite comprising CNTs with a nominal diameter of 60 nm that has been processed at 700 °C in Ar.

sitic oxidative process recorded at the same voltage by CV. This plateau can be partially suppressed if a higher cycling rate (C/5 or C/2) is applied, which allows a shorter period of time for the oxidation process to occur.

The discharge capacity retention vs. cycle numbers for an ordered 3D CNT/$LiCoPO_4$ composite comprising CNTs with a nominal diameter of 60 nm, a conventional carbon black/$LiCoPO_4$ composite, and a CNT/$LiCoPO_4$ composite with stochastically oriented CNTs were studied (Figure 14). The best electrochemical performance was found for the stochastically ordered CNT/$LiCoPO_4$ composite, followed by conventional carbon black/$LiCoPO_4$ and ordered 3D CNT/$LiCoPO_4$ composites containing CNTs with a nominal diameter of 60 nm.

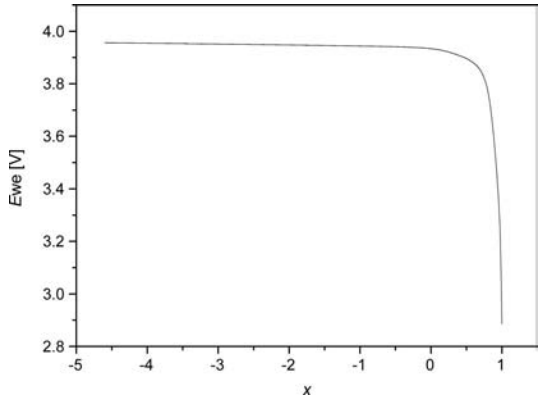

Figure 14. Galvanostatic cycling measured at C/10 for a 3D CNT/$LiCoPO_4$ composite comprising CNTs with a nominal diameter of 200 nm.

The 3D CNT/$LiCoPO_4$ composites containing 60 nm CNTs show a higher electrochemical stability during charging compared to composites containing 200 nm CNTs. Covering the CNTs with $LiCoPO_4$ seems to protect them partially from strong oxidation during the first discharge cycle at ca. 4.9 V. Formation of large $LiCoPO_4$ particle agglomerates inside the ordered 3D CNT/$LiCoPO_4$ composite (shown in Figure 9) obviously prevents effective Li diffusion and therefore reduces the observed electrochemical capacity values.

Finally, we studied the cycle stability of the 3D CNT/$LiCoPO_4$ composites containing CNTs with a nominal diameter of 60 nm but different loadings of $LiCoPO_4$ olevin (Figure 15). Loading of the CNT structures with precursor concentrations between 0.1 and 0.3 M results in a nonlinear dependency of the capacity retention as a function precursor concentration. A 0.1 M precursor solution provides a small amount of the active $LiCoPO_4$ material that is distributed on the surface of the CNTs within the array. The resultant composite shows good cycle stability. A higher concentration of precursor solution (0.3 M) provides an excess of $LiCoPO_4$ and leads to the formation of more uniform agglomerates and a more dense tethering of the active material onto the 3D CNT surface, this causes an increase in the cycle stability (Figure 16).

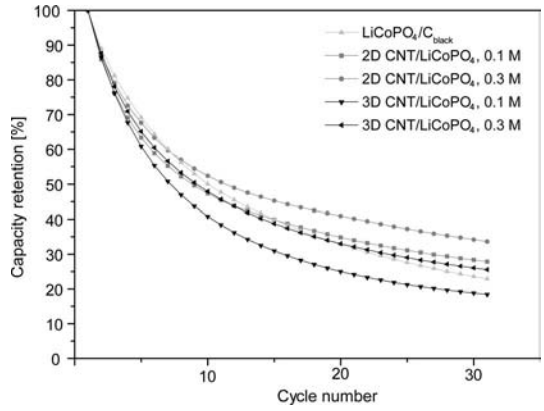

Figure 15. Charge/discharge retention capacity (%) vs. cycle number for 3D CNT/$LiCoPO_4$ and stochastically arranged CNT/$LiCoPO_4$ composites comprising CNTs with a nominal diameter of 60 nm but with different concentrations of active $LiCoPO_4$ (0.1 M and 0.3 M precursor sol). Also shown are data for carbon black/$LiCoPO_4$. Galvanostatic experiments were performed between 3 and 5 V at a rate of C/10.

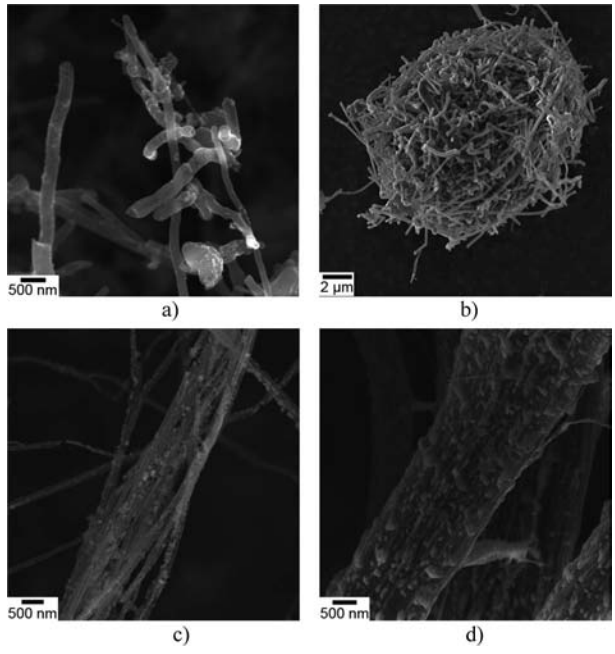

Figure 16. SEM micrographs of stochastically arranged CNT/$LiCoPO_4$ (a and b) and 3D ordered CNT/$LiCoPO_4$ composites (c and d) prepared with 0.1 M (a and c) and 0.3 M (b and d) precursor solutions. Note that for the higher $LiCoPO_4$ loading pronounced agglomeration and bundeling of the CNT/$LiCoPO_4$ composite is observed.

The difference in the electrochemical performance of the various CNT/$LiCoPO_4$ composites studied might be due to a combination of different effects. The observed size variance (inhomogeneity) of the $LiCoPO_4$ nanoparticles tethered onto the CNT surface and/or the formation of large $LiCoPO_4$ particle agglomerates inside the MWCNTs of the CNT/$LiCoPO_4$ composites, certainly have a strong impact on the electrochemical performance of the composite, as well as on the final temperature necessary for the calci-

nation of the $LiCoPO_4$ olevin. Nonoptimal loading of the conducting CNT array structure and the variable range of $LiCoPO_4$ particle sizes, might further prevent effective Li diffusion within the conducting CNT array structure and therefore reduce the capacity values. Nevertheless, the use of a nanosized composite cathode structures, such as CNT/nanoscale $LiCoPO_4$, is certainly desirable since the diffusion pathways for the Li ions within the conducting carbon cathode material is significantly shortened relative to those in other composites, thus increasing the diffusion rate and enabling better kinetic transport conditions. The better electrochemical performance of the stochastically arranged CNTs in the MWCNT/$LiCoPO_4$ composite when compared to the ordered 3D MWCNT/$LiCoPO_4$ composite architecture can be explained by the better connection, and thus electronic conductivity, between the $LiCoPO_4$ nanoparticles and the stochastically ordered CNTs in the former composite. This enhanced connectivity may arise during the post annealing process of the $LiCoPO_4$ olevin particles that is conducted at 700 °C for the MWCNT/$LiCoPO_4$ composite comprising stochastically arranged CNTs. This process may allow for a more intimate association of the $LiCoPO_4$ particles with the CNT surfaces when compared to the particle-surface interactions in the more rigid and compact ordered 3D CNT/$LiCoPO_4$ composite structure. Recently, a study of a composite composed of stochastically distributed CNT networks interlaced into a 3D $LiFePO_4$ matrix revealed a significantly improved specific capacity and rate performance for this material in comparison to unmodified CNT free porous $LiFePO_4$.[32]

To provide additional evidence for these findings, we performed studies of the electrochemical performance of $LiFePO_4$ particles (derived from a polyol-sol-gel route), and tethered these particles onto stochastically distributed MWCNTs in order to prove independently that a significantly enhanced performance of such CNT/$LiFePO_4$ composites occurs when the $LiCoPO_4$ olevine particle size is properly adjusted to complement the size of the CNTs. The capacity values increased up to 133 mA hg^{-1} for pure $LiFePO_4$, and even up to 154 mA hg^{-1} (91 % of the theoretical capacity at a discharge rate of 0.1/C) for the $LiFePO_4$/CNT composites in which the CNTs were further functionalized prior to tethering of the phosphoolevin particles.[32] Figure 17 shows SEM micrographs of such nanoscale $LiFePO_4$ particles derived from a polyol process with tetra ethylene glycol as the solvent, before and after deposition of these particles onto the stochastically arranged MWCNTs (see Figure 17, parts a and b, respectively). Both samples were processed at 500 °C for 12 h to yield the active olivine material from the sol particles. The CNTs are homogeneously covered with agglomerates of small particles that show pronounced sintering caused by the long term thermal annealing process that was, however, necessary in order to obtain the active phosphoolevin particles from the as-prepared nanoparticles.[33] Accordingly, a higher processing temperature of 800 °C drastically lowered the charging capacity of the $LiFePO_4$/CNT composite to only 59 mA hg^{-1}. This might be due to extensive sintering of the $LiFePO_4$ particles resulting in large micron-sized aggregates that strongly inhibit the efficient diffusion of the Li ions, and thus this type of treatment should be avoided. These findings point towards the importance of optimal matching of the active olevin particle size with the CNT diameter in order to obtain optimal electrochemical performance from the resultant composites.

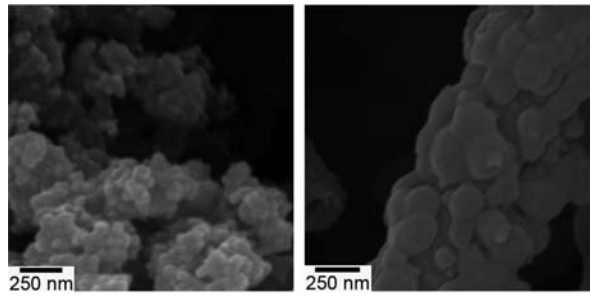

Figure 17. (a) SEM micrographs of bare $LiFePO_4$ particles obtained by a polyol approach; (b) the same material deposited from solution onto the surface of stochastically arranged MWCNTs. The olevin particles are covering the surface of the CNTs fairly homogeneously, and show a morphology based on the interconnection of the particles.

Conclusions

Hybrid materials composed of $LiCoPO_4$ and MWCNTs, namely, stochastically arranged MWCNT/$LiMPO_4$ and ordered 3D MWCNT/$LiCoPO_4$ composites were synthesized by the combination of a templated CVD technique and a wet chemical impregnation by a sol-gel based method. Ordered 3D CNT monoliths comprising CNTs with nominal diameters of either 60 nm or 200 nm were synthesized withPAOX templates in a catalyst free CVD process. The 3D CNT monoliths could be surface functionalized without destroying the ordered 3D CNT arrangement. An ethanol based sol route, together with an organic phosphate, was used to tether nanoscale phosphoolivine particles onto the disordered and ordered 3D CNT arrays. Electrochemical measurements on the obtained composites revealed a significant enhancement of the electrochemical performances of these materials in comparison with the isolated $LiCoPO_4$ phosphoolivine phase that was obtained under analogous conditions. The electrochemical measurements also demonstrated the good electrochemical stability of the ordered 3D CNT/$LiCoPO_4$ composites during cycling of the battery test cells. Future studies will focus on improving the homogeneity of the electroactive $LiCoPO_4$ particles, which may be achieved by optimizing the nanoparticle stability and growth. Furthermore, additional studies will involve the modification of the deposition process to ensure that the particles infiltrate the void space within the 3D CNT monolith structures more effectively. This will certainly lead to even higher loadings of the 3D CNT structures than already achieved, and a further improvement in the long term stability of the 3D CNT/$LiCoO_4$ composite cathodes during cycling.

Experimental Section

Synthesis and Functionalization of an Ordered 3D CNT Monolithic Structure: Ordered 3D CNT monoliths were prepared by a template assisted chemical vapour deposition (CVD) process. Porous aluminium oxide (PAOX) templates about 2 cm^2 in size and with pore diameters of approximately 60 nm (+/– 5 nm) were used in this process.[22] Ethylene (10 sccm) was the carbon source and Ar (10 sccm) was the diluent carrier gas. The depositions were performed at 800 °C for 20 min without an additional catalyst. After the CVD process, the PAOX template was wet etched with HF to obtain a freestanding 3D CNT monolith with one dimensionally arranged CNTs. A unique feature of this process is that the resultant CNTs are sandwiched between thin carbon layers. The top carbon layer can be removed by placing the CNT block in an oxygen plasma for 10–15 min (Plasma cleaner, Fa. Diener Electronics, type Femto). The thus obtained block arrangements with nominal pore diameters of 60 nm (±5 nm) are composed of well aligned CNTs, the lengths of which are determined by the thickness of the alumina template. The CNTs were unhinged from the block structure for analytical purposes by long term ultrasonification of the 3D CNT blocks. Chemical functionalization of the 3D CNT block arrays was achieved by treatment with conc. HNO_3 at 70 °C and at 140 °C. After treatment, suspensions of the 3D CNT arrays in HNO_3 were diluted with deionized water, filtered, washed several times with water then ethanol and dried at 110 °C in air.

Synthesis of $LiCoPO_4$: $LiNO_3$ (99.99%, Aldrich), $Co(NO_3)_2{\cdot}6H_2O$ (98% Alfa Aesar), and $P(OC_2H_5)_3$ (98%, Alfa Aesar) were used in the synthesis of $LiCoPO_4$. Firstly, triethyl phosphite was diluted in ethanol. Stoichiometric amounts of cobalt and lithium nitrates in an ethanol solution (0.1 M) were added dropwise to the triethyl phosphite solution. The presence of hydrate water in the nitrate salts led to the immediate formation of a sol. The solution was left for a period of 24–72 h. The solvents were then evaporated at 60 °C under flowing Ar until a viscous liquid was obtained. Further drying of the viscous liquid at 60 °C resulted in a white gel. The gel was calcinated at 700 °C under flowing Ar.

Materials Characterization: IR spectroscopic measurements were carried out with a Nicolet FTIR spectrometer. X-ray powder diffraction (XRD) of the composites were performed with a StadiP instrument from StadiP, Stoe & Cie GmbH, Darmstadt (flat specimen, transmission mode) operating with Co-$K_{\alpha 1}$ radiation and equipped with a Ge(111) monochromator. The diffraction patterns were identified by comparison with data in the ICDD database. SEM investigations were performed with a Philips XL 30 FEG microscope operating at 20 keV.

Electrochemical Measurements: Electrochemical studies were carried out with a multichannel potentiostatic–galvanostatic system VMP (Perkin–Elmer Instruments, USA). Swagelok-type cells were assembled in an argon-filled dry box with water and oxygen contents of less than 1 ppm. The 3D CNT/$LiCoPO_4$ composite cathodes containing 0.1–0.2 mg of the electroactive Co compound were pressed onto an Al-mesh (8 mm diameter, pressure < 5 bar) and dried at 100 °C under vacuum for ca. 10 h. For comparison, powders of $LiCoPO_4$, and carbon black with polyvinylidene fluoride (PVdF) as a polymer binder in an 85:10:5 weight ratio with the addition of *N*-methyl-1,2-pyrrolidone, as well as a disordered MWCNT/$LiCoPO_4$ composite were also investigated as cathode materials. The average diameter of the disordered MWCNTs was about 70–100 nm. The anode was made of lithium metal and a mixture containing 1 M $LiPF_6$ in ethylene carbonate/dimethyl carbonate (EC:DMC, 1:1) was the electrolyte. A glass fiber separator was placed between the anode and cathode sides of the cell. Cyclic voltammetry was carried out with a scan rate of 0.1 mV/s between 3.0 and 5.0 or 5.3 V. Galvanostatic measurements were performed at a rate of C/10 and between 3.0 and 5.0 V.

Acknowledgments

This work was supported by the Deutsche Forschungsgemeinschaft (DFG) within the priority program SPP 1181 (JA859/14, SCHN375/16, EH183/3).

[1] *Advanced Micro & Nanosystems, Carbon Nanotube Devices* (Ed.: C. Hierold), vol. 8, Wiley-VCH, Weinheim, Germany, **2008**.
[2] J. Khanderi, R. C. Hoffmann, J. J. Schneider, *Nanoscale* **2010**, *2*, 613.
[3] A. L. M. Reedy, M. M. Shaijumon, S. R. Gowda, P. M. Ajayan, *Nano Lett.* **2009**, *9*, 1002.
[4] a) D. Eder, *Chem. Rev.* **2010**, *110*, 1348; b) W.-D. Zhang, B. Xu, L.-C. Jiang, *J. Mater. Chem.* **2010**, *20*, 6383.
[5] A. Popp, J. J. Schneider, *Angew. Chem. Int. Ed.* **2008**, *47*, 8958.
[6] a) J. Khanderi, R. C. Hoffmann, J. Engstler, J. J. Schneider, J. Arras, P. Claus, G. Cherkashinin, *Chem. Eur. J.* **2010**, *16*, 2011; b) J. P. Khanderi, C. Contiu, J. Engstler, R. C. Hoffmann, J. J. Schneider, A. Drochner, H. Vogel, *Nanoscale* **2011**, DOI: 10.1039/c0nr00723d.
[7] B. L. Ellis, K. T. Lee, L. F. Nazar, *Chem. Mater.* **2010**, *22*, 691.
[8] X.-L. Wu, L.-Y. Jiang, F.-F. Cao, Y.-G. Guo, L.-J. Wan, *Adv. Mater.* **2009**, *21*, 2710.
[9] A. K. Padhi, K. S. Nanjundaswamy, J. B. Goodenough, *J. Electrochem. Soc.* **1997**, *144*, 1188.
[10] A. S. Andersson, B. Kalska, L. Haggstrom, J. O. Thomas, *Solid State Ionics* **2000**, *130*, 41.
[11] Z. Chen, Y. Qin, K. Amien, Y.-K. Sun, *J. Mater. Chem.* **2010**, *20*, 7607.
[12] J. Barker, M. Y. Saidi, J. L. Swoyer, *Electrochem. Solid-State Lett.* **2003**, *6*, A53.
[13] R. Dominko, J. M. Goupil, M. Bele, M. Gaberscek, M. Remskar, D. Hanzel, J. Jamnik, *Electrochem. Solid-State Lett.* **2005**, *152*, A858.
[14] J. Moskon, R. Dominko, M. Gaberscek, R. Cerc-Korosec, J. Jamnik, *J. Electrochem. Soc.* **2006**, *153*, A1805.
[15] K. Zaghib, J. Shim, A. Guerfi, P. Charest, K. A. Striebel, *Electrochem. Solid State Lett.* **2005**, *8*, A204.
[16] G. Meng, F. Han, X. Zhao, B. Chen, D. Yang, J. Liu, Q. Xu, M. Kong, X. Zhu, Y. J. Jung, Y. Yang, Z. Chu, M. Ye, S. Kar, R. Vajtai, P. M. Ajayan, *Angew. Chem. Int. Ed.* **2009**, *48*, 7166.
[17] Q. Lin, J. N. Harb, *J. Electrochem. Soc.* **2004**, *151*, A1115.
[18] B. J. Landi, R. A. Dileo, C. M. Schauerman, C. D. Cress, M. J. Ganter, R. P. Raffaelle, *J. Nanosci. Nanotechnol.* **2009**, *9*, 3406.
[19] W.-J. Yu, P.-X. Hou, L. L. Zhang, F. Li, C. Liu, H.-M. Cheng, *Chem. Commun.* **2010**, *46*, 8576.
[20] Y. Wang, Y. Wang, E. Hososno, K. Wang, H. Zhou, *Angew. Chem.* **2008**, *120*, 7571.
[21] X. Li, F. Kang, X. Bai, W. Shen, *Electrochem. Commun.* **2007**, *9*, 663.
[22] M. S. Bhuvaneswari, N. N. Bramnik, D. Ensling, H. Ehrenberg, W. Jaegermann, *J. Power Sources* **2008**, *180*, 553.
[23] a) J. J. Schneider, J. Engstler, K. P. Budna, C. Teichert, S. Franzka, *Eur. J. Inorg. Chem.* **2005**, 2352; b) J. J. Schneider, J. Engstler, *Eur. J. Inorg. Chem.* **2006**, 1723.
[24] J. J. Schneider, N. I. Maximova, J. Engstler, R. Joshi, R. Schierholz, R. Feile, *Inorg. Chimica Acta* **2008**, *361*, 1770.
[25] M. Pashchanka, R. C. Hoffmann, A. Gurlo, J. J. Schneider, *J. Mater. Chem.* **2010**, *20*, 8311.

[26] O. Yilmazoglu, A. Popp, O. Kaldirim, D. Pavlidis, J. J. Schneider, *Chem. Commun.* **2009**, *45*, 3205.
[27] P. Mahanandia, J. J. Schneider, M. Kahneft, B. Stühn, T. P. Peixoto, B. Drossel, *Phys. Chem. Chem. Phys.* **2010**, *12*, 4407.
[28] A. Sarapulova, N. N. Bramnik, D. Mikhailova, L. A. Schmitt, S. Oswald, H. Ehrenberg, manuscript in preparation.
[29] J. L. Shui, Y. Yu, X. F. Yang, C. H. Chen, *Electrochem. Commun.* **2006**, *8*, 1087.
[30] K. Amine, H. Yasuda, M. Yamachi, *Electrochem. Solid-State Lett.* **2000**, *3*, 178.
[31] N. N. Bramnik, K. Nikolowski, D. M. Trots, H. Ehrenberg, *Solid-State Lett.* **2008**, *11*, A89.
[32] Y. Zhou, J. Wang, Y. Hu, R. O'Hayre, Z. Shao, *Chem. Commun.* **2010**, *46*, 7151.
[33] N. N. Bramnik, K. Nikolowski, C. Baehtz, K. G. Bramnik, H. Ehrenberg, *Chem. Mater.* **2007**, *19*, 908.

Received: March 2, 2011
Published Online: August 19, 2011

